STUDY OF THE GRAVITATIONAL CAPTURE AT MERCURY IN THE ELLIPTIC RESTRICTED THREE-BODY PROBLEM

Yi Qi [(1)], **Shijie Xu** [(2)], **and Rui Qi** [(3)]

[(1)] *PhD Candidate, Department of Aerospace Engineering, School of Astronautics, Beihang University, Beijing, 100191, China, lushenqiyi@gmail.com*

[(2)] *Professor, Department of Aerospace Engineering, School of Astronautics, Beihang University, Beijing, 100191, China, starsjxu@163.com*

[(3)] *Lecturer, School of Aerospace Engineering, Beijing Institute of Technology, Beijing, 100081, China, qirui@bit.edu.cn*

Abstract: *Gravitational capture is an important characteristic of N-body (N≥3) dynamical systems. In this paper, the gravitational capture at Mercury is investigated under the frame of elliptic restricted three body problem (ER3BP). A new parameter k, the corrected ratio of the radial force, is proposed to analyze the influence of radial force on the capture eccentricity in the ER3BP. The parametric analysis elucidates the influences on the corrected ratio k and tangential force. The minimum capture eccentricity and the corrected minimum capture eccentricity are respectively introduced under the time-of-flight and corrected ratio. By numerical computation, we find the vicinity of perihelion is the optimal location for the gravitational capture, and the global minimum of two kinds of minimum capture eccentricity are both distributed on two special regions of the sphere of capture, which denote the optimal regions for gravitational capture. Finally, using the results presented, we design some capture trajectories for potential Mercury missions.*

Keywords: *Gravitational Capture, Mercury Mission, Elliptic Restricted Three Body Problem, Trajectory Design.*

1. Introduction

The gravitational capture is a useful phenomenon in the design of low energy transfer (LET) orbit and has been applied in some deep space missions. The first example was the rescue of the Japanese lunar probe Hiten in 1991 [1]. After that, SMART-1 achieved the capture at Moon via the gravitational capture [2]. Recently, NASA's GRAIL mission exploited similar concept to reach the Moon [3]. For the interplanetary transfer, gravitational capture was also applied to design the trajectory of ESA's BepiColombo mission [4], which was aimed to explore Mercury.

Gravitational capture occurs, when the orbital eccentricity of motion around one celestial body is altered from greater than 1 to less than 1 without use of any propulsive system. Even though the gravitational capture is not permanent capture, it can effectively reduce the fuel consumption comparing with Hohmann transfer [5, 6, 7].

The first research in this field can trace back to 1987, when Belbruno proposed the Weak Stability Boundary (WSB) theory to achieve lunar capture without braking [5]. Further studies were conducted by Belbruno and Miller [8], Krish et al [9]. They all studied missions of the Earth-to-Moon LET and used this technique to save fuel during inserting a spacecraft into its final orbit around the Moon. After that, some studies considering the time requirement for this

transfer appeared in the literature [10, 11]. Considering the WSB, temporary capture and the LETs, Fantino et al. discussed the role played by the invariant manifolds in each of them [12]. As the research continued, more complicated models were investigated. The gravitational capture based on bicircular model (BCM) in restricted four body problem (R4BP) can be available in the literatures [11, 13]. The effect of planetary eccentricity on ballistic capture in the elliptic restricted three body problem (ER3BP) was also investigated [14, 15]. Using the concept of stable sets, Hyeraci and Topputo proposed a systematic method to design ballistic capture orbits upon planet arrival in interplanetary transfers in the ER3BP [16]. Those researches about ER3BP, however, just involved the planar capture problem, and the results could not be extended to the spatial situation of the capture directly.

In this paper, several spatial issues of gravitational capture at Mercury in the ER3BP are studied. Firstly, the basic theories of the problem and the gravitational capture are introduced. Then, to derive capture eccentricity in the ER3BP, the corrected ratio of the radial force is proposed via the analysis of the mechanical characters in the space near Mercury. Numerical study displays the influences of different factors on the corrected ratio. Because of the importance of the eccentricity, the minimum capture eccentricity in the ER3BP is investigated. Finally, applying the results obtained in this paper, we construct some gravitational capture trajectories of Mercury.

2. Basic Theory

2.1. The Elliptic Restricted Three Body Problem

The ER3BP is shown in Fig. 1. It is described in the inertial frame, in which m_1, m_2 and m_3 represent the Sun, Mercury and spacecraft respectively. In the ER3BP, the mass of the spacecraft is supposed to be negligible, and only the effects of the two primary bodies are considered. Therefore the motion of the spacecraft is influenced by the attraction of the Sun and Mercury, but the motion of two primary bodies cannot be affected by the spacecraft. Besides, the ER3BP is built on the hypothesis that the motion of two primary bodies is restricted. Specifically, the Sun and Mercury are in elliptic motion about the Sun–Mercury barycenter (SMB).

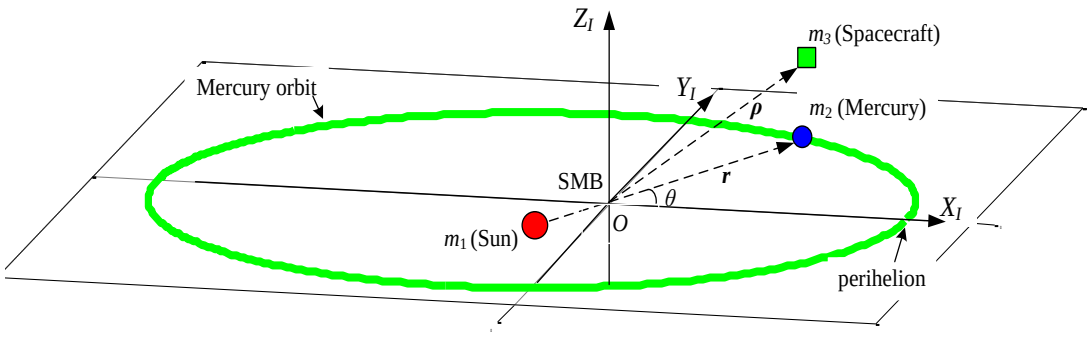

Figure 1. The ER3BP in the inertial frame

In the Fig.1， the origin O is fixed at the SMB and X_I axis points to the perihelion. Mercury orbital plane coincides with X_IOY_I plane. The vector $\boldsymbol{r}$ points to Mercury from the Sun, and $\boldsymbol{\rho}$ is the position vector of spacecraft w.r.t the SMB. θ is the angle between the X_I axis and the

vector $\boldsymbol{r}$, that is Mercury true anomaly. The relative position vectors of the bodies can be expressed as

$$\boldsymbol{r}_{13} = \boldsymbol{\rho} + \mu\boldsymbol{r} \tag{1a}$$

$$\boldsymbol{r}_{23} = \boldsymbol{\rho} - (1-\mu)\boldsymbol{r} \tag{1b}$$

where $\mu = \dfrac{m_2}{m_1 + m_2}$, is the ratio of Mercury's mass to the sum of masses of the Sun and Mercury.

Under the inertial frame, the equation of motion of the spacecraft can be expressed as follows:

$$\ddot{\boldsymbol{\rho}} = -Gm_1 \frac{\boldsymbol{\rho} + \mu\boldsymbol{r}}{\left|\boldsymbol{\rho} + \mu\boldsymbol{r}\right|^3} - Gm_2 \frac{\boldsymbol{\rho} - (1-\mu)\boldsymbol{r}}{\left|\boldsymbol{\rho} - (1-\mu)\boldsymbol{r}\right|^3} \tag{2}$$

where G is the universal gravitational constant.

Utilizing the rotation matrix C_I^R, the equations of motion can be transformed into the Sun-Mercury rotating frame. The origin is fixed at the SMB. The x axis points to Mercury from the Sun. So we can obtain the expression of C_I^R.

$$C_I^R = \begin{bmatrix} \cos\theta & \sin\theta & 0 \\ -\sin\theta & \cos\theta & 0 \\ 0 & 0 & 1 \end{bmatrix} \tag{3}$$

Substituting Eq. 3 into Eq. 2 yields

$$\frac{d^2(C_R^I\boldsymbol{\rho}^R)}{dt^2} = -Gm_1 \frac{C_R^I(\boldsymbol{\rho}^R + \mu\boldsymbol{r}^R)}{\left|\boldsymbol{\rho}^R + \mu\boldsymbol{r}^R\right|^3} - Gm_3 \frac{C_R^I(\boldsymbol{\rho}^R - (1-\mu)\boldsymbol{r}^R)}{\left|\boldsymbol{\rho}^R - (1-\mu)\boldsymbol{r}^R\right|^3} \tag{4}$$

where the vectors $\boldsymbol{r}^R$ and $\boldsymbol{\rho}^R$ are denoted in the rotating frame $\mathbb{F}_R$, so $\boldsymbol{r} = C_R^I\boldsymbol{r}^R$, $\boldsymbol{\rho} = C_R^I\boldsymbol{\rho}^R$.

To simplify the form of the equation, nondimensionalization is applied. The unit length l_N is set as r, the length of the vector $\boldsymbol{r}$. The unit time t_N is set as $\dfrac{T_{EM}}{2\pi} = \sqrt{\dfrac{a}{G(m_1 + m_2)}}$, where a and T_{EM} are the semi-major axis and the period of Sun-Mercury system respectively. As r is fixed in nondimensional rotating frame, then Eq. 4 becomes

$$\begin{aligned}&\ddot{\boldsymbol{\rho}}^N + 2\left(C_I^R\dot{C}_R^I + \frac{\dot{r}}{r}\right)\dot{\boldsymbol{\rho}}^N + \left(\frac{\ddot{r}}{r} + 2\frac{\dot{r}}{r}C_I^R\dot{C}_R^I + C_I^R\ddot{C}_R^I\right)\boldsymbol{\rho}^N \\ &\quad = -(1-\mu)\left(\frac{a}{r}\right)^3 \frac{\boldsymbol{\rho}^N + \mu\boldsymbol{r}^N}{\left|\boldsymbol{\rho}^N + \mu\boldsymbol{r}^N\right|^3} - \mu\left(\frac{a}{r}\right)^3 \frac{\boldsymbol{\rho}^N - (1-\mu)\boldsymbol{r}^N}{\left|\boldsymbol{\rho}^N - (1-\mu)\boldsymbol{r}^N\right|^3}\end{aligned} \tag{5}$$

where $\boldsymbol{r}^N = \dfrac{\boldsymbol{r}^R}{r}$, $\boldsymbol{\rho}^N = \dfrac{\boldsymbol{\rho}^R}{r}$.

Besides, we can derive

$$C_I^R\dot{C}_R^I = \dot{\theta}\begin{bmatrix}0 & -1 & 0\\ 1 & 0 & 0\\ 0 & 0 & 0\end{bmatrix} \tag{6a}$$

$$C_I^R\ddot{C}_R^I = \begin{bmatrix}-\dot{\theta}^2 & -\ddot{\theta} & 0\\ \ddot{\theta} & -\dot{\theta}^2 & 0\\ 0 & 0 & 0\end{bmatrix} \tag{6b}$$

Since the motion of two primaries is considered elliptic, then the following relation can be used:

$$\dot{\theta} = \frac{(1+e\cos\theta)^2}{\sqrt{(1-e^2)^3}} \tag{7a}$$

$$\ddot{\theta} = -2\dot{\theta}^2\eta_1 \tag{7b}$$

$$\frac{\dot{r}}{r} = \dot{\theta}\eta_1 \tag{7c}$$

$$\frac{\ddot{r}}{r} = \dot{\theta}^2\eta_2 \tag{7d}$$

where e is the eccentricity of Mercury orbit and equal to 0.20563, and

$$\eta_1 = \frac{e\sin\theta}{1+e\cos\theta} \tag{8a}$$

$$\eta_2 = \frac{e\cos\theta}{1+e\cos\theta} \tag{8b}$$

To simplify the form of the equation, we substitute the vectors $\boldsymbol{r}$ and $\boldsymbol{\rho}$ for the vector $\boldsymbol{r}^N$ and $\boldsymbol{\rho}^N$. Using Eqs. 5 ~ 8 and the definition of η_3,

$$\eta_3 = \frac{1}{1+e\cos\theta} = 1-\eta_2 \tag{9}$$

The final equation of motion of spacecraft in the nondimensional Sun-Mercury rotating frame is expressed as

$$\begin{pmatrix} \ddot{x} \\ \ddot{y} \\ \ddot{z} \end{pmatrix} = \begin{pmatrix} -2\dot{\theta}(\eta_1\dot{x}-\dot{y})+\eta_3\dot{\theta}^2 x \\ -2\dot{\theta}(\eta_1\dot{y}+\dot{x})+\eta_3\dot{\theta}^2 y \\ -2\dot{\theta}\eta_1\dot{z}-\eta_2\dot{\theta}^2 z \end{pmatrix} - (1-\mu)\left(\frac{a}{r}\right)^3 \frac{\boldsymbol{\rho}+\mu\boldsymbol{r}}{|\boldsymbol{\rho}+\mu\boldsymbol{r}|^3} - \mu\left(\frac{a}{r}\right)^3 \frac{\boldsymbol{\rho}-(1-\mu)\boldsymbol{r}}{|\boldsymbol{\rho}-(1-\mu)\boldsymbol{r}|^3} \tag{10}$$

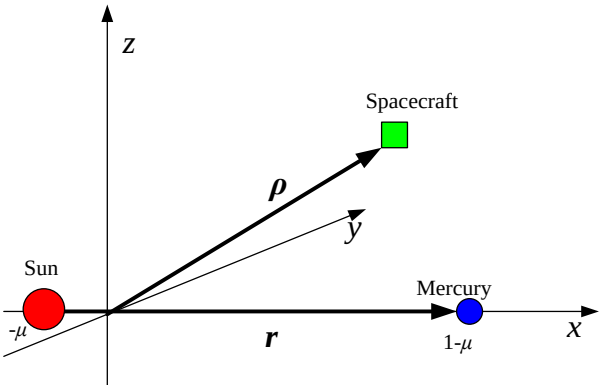

Figure 2. The ER3BP in nondimensional rotating frame

For details we can see Fig. 2, where the vectors $\boldsymbol{\rho}$ and $\boldsymbol{r}$ will be $\boldsymbol{\rho} = (x, y, z)^T$, $\boldsymbol{r} = (1, 0, 0)^T$, respectively.

2.2. Gravitational Capture

In two-body model, the energy E of spacecraft or the eccentricity e_c of the capture orbit determines the shape of orbit. If $E > 0$ or $e_c > 1$, the orbit is an open hyperbolic orbit. If E=0 or e_c=1, the orbit is an open parabolic orbit. If $E < 0$ or $e_c < 1$, the orbit is a closed elliptical orbit. E can be written as: $E = V^2/2 - \mu/d$, where d and V are the distance and the velocity of the spacecraft with respect to the celestial body, respectively, and μ is the gravitational parameter of the celestial body. In the ER3BP, if the spacecraft is in the vicinity of one primary body, the gravitation of that body is dominant, while the influences from other bodies are relatively less important. Therefore the concept of energy E and the eccentricity e can still be used to study the orbital character in the ER3BP. Different from that in two-body model, E and e_c are time-

varying in the ER3BP. Hence the energy E can be alternated from positive to negative, or the orbital eccentricity e_c can be alternated from greater than 1 to less than 1, which both means that the transient orbit can be alternated from open orbit to closed orbit. This phenomenon is called the gravitational capture. Of particular note is that the gravitational capture is temporary capture, but if spacecraft is braked properly during this temporary capture, a permanent capture will be accomplished with less fuel consumption [5, 6, 7].

The gravitational capture at Mercury is shown in Fig. 3. The spacecraft is captured temporarily at the capture point after it enters the region of influence from outside. The distance from the capture point to the barycenter of Mercury is d, and the velocity of the spacecraft is V. Existing literatures defined the region of the influence in different ways, such as the SOI [17] and Hill sphere [18]. In this paper, we adopt the definition of the SOI proposed by Jehn et al. [4], which consider the radius of the SOI is 300000 km.

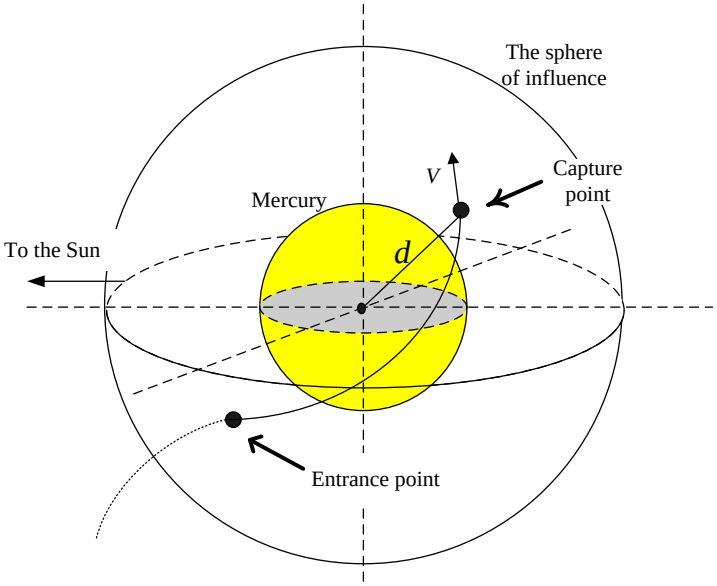

Figure 3. The gravitational capture at Mercury

If the direction of the velocity vector of the spacecraft is perpendicular to the line that links the spacecraft to the barycenter of Mercury, there is a relationship in two-body model as follows

$$v = \sqrt{\frac{\mu_m}{d}(1+e_c)} \tag{11}$$

where v is the velocity of the spacecraft at capture point, d is the distance from the capture point to the barycenter of Mercury, e_c is the eccentricity of the capture orbit, and μ_m is the gravitational parameter of Mercury. If $0 < e_c < 1$, the capture point is periherm, and if $e_c < 0$, the capture point is apoherm.

3. Mechanics Analysis in the Space near Mercury

3.1. Radial Force and Tangential Force

Adequate knowledge about the mechanical property of the space near Mercury can help us understand the gravitational capture at Mercury. In the Sun-Mercury rotating frame, acceleration decomposition is applied to analyze the dynamics of spacecraft as follows,

$$\boldsymbol{a}_r = \boldsymbol{a}_a - \boldsymbol{a}_e - \boldsymbol{a}_c \tag{12}$$

where $\boldsymbol{a}_r$ is the relative acceleration of spacecraft in the rotating frame, $\boldsymbol{a}_a$ is the absolute acceleration, $\boldsymbol{a}_e$ is the translational acceleration, and $\boldsymbol{a}_c$ is the Coriolis acceleration. Same as Sect.2.1, we apply nondimensionalization to the mechanical quantity in analysis. And the definition of the length unit and the time unit is also same as that in Sect.2.1. The unit length is time-varying because the eccentricity e of Mercury orbit is not 0. This influence will be coupled to each accelerations in Eq. 12. Using Eq. 10, we can obtain the expression of $\boldsymbol{a}_r$ in the nondimensional Sun-Mercury rotating frame.

$$\boldsymbol{a}_r = \left[-(1-\mu)\left(\frac{a}{r}\right)^3 \frac{\boldsymbol{\rho}+\mu\boldsymbol{r}}{\left|\boldsymbol{\rho}+\mu\boldsymbol{r}\right|^3} - \mu\left(\frac{a}{r}\right)^3 \frac{\boldsymbol{\rho}-(1-\mu)\boldsymbol{r}}{\left|\boldsymbol{\rho}-(1-\mu)\boldsymbol{r}\right|^3} \right] + \begin{pmatrix} \eta_3\dot{\theta}^2 x \\ \eta_3\dot{\theta}^2 y \\ -\eta_2\dot{\theta}^2 z \end{pmatrix} - 2\dot{\theta}\begin{pmatrix} \eta_1\dot{x}-\dot{y} \\ \eta_1\dot{y}+\dot{x} \\ \eta_1\dot{z} \end{pmatrix} \tag{13}$$

where the terms in the first square bracket are the expansion of $\boldsymbol{a}_a$, including the gravity acceleration of the Sun and Mercury, respectively. The terms in the second bracket is the centrifugal acceleration, $-\boldsymbol{a}_e$. The terms in the last bracket is the Coriolis acceleration, $\boldsymbol{a}_c$. As we can see from Eq. 13, a/r, η_1 and η_2 are the coupling terms of *e*.

On the other hand, from Eq. 13, the position $\boldsymbol{\rho}$ of spacecraft only affects the terms in the first two brackets, the velocity $\dot{\boldsymbol{\rho}}$ of spacecraft only affects the terms in the last bracket. But the influences of θ appear in all terms in Eq. 13.

We define the direction from the spacecraft to the barycenter of Mercury and the direction of the spacecraft's velocity as the radial direction and the tangential direction, respectively. To investigate the capture in the space near Mercury, the acceleration $\boldsymbol{a}_r$ is decomposed along the radial direction and the tangential direction. Then we obtain the radial acceleration $\boldsymbol{a}_r^r$ and the tangential acceleration $\boldsymbol{a}_r^t$. The radial acceleration $\boldsymbol{a}_r^r$ in the ER3BP is equivalent to the gravitational acceleration in two-body model, so it is directly related to the gravitational capture. And the greater the radial acceleration is, the easier the gravitational capture will be. The tangential acceleration $\boldsymbol{a}_r^t$ is considered to affect the braking at the capture point. The velocity increment $\Delta\boldsymbol{v}$ caused by the tangential acceleration has the following expression

$$\Delta\boldsymbol{v} = \boldsymbol{a}_r^t \Delta t \tag{14}$$

where Δt is braking time. Apparently, the tangential acceleration $\boldsymbol{a}_r^t$ in the opposite direction to the velocity $\boldsymbol{v}$ facilitates capture.

According to the mechanics analysis shown above, we find except the gravity acceleration of Mercury, that all kinds of force could have component in the tangential direction, even the Coriolis force. But for the radial direction, each kinds of force could have component. Hence the mechanical circumstance in the ER3BP is more complex than that in two-body model, where only the radial acceleration of the Mercury gravity exists.

3.2. Corrected Ratio of the Radial Force

In this paper, we suppose the capture point is periherm. If the velocity of spacecraft at capture point is v_p and the distance from the capture point to the barycenter of Mercury is r_p. Eq. 11 in Sect.2.2 can be rewritten as

$$v_p = \sqrt{\frac{\mu_m}{r_p}(1+e_c)} \tag{15}$$

Eq. 15 is established in two-body model, but not applicable in the ER3BP. To solve this problem, we propose a new parameter *k*, the corrected ratio of the radial force. It describes the proportion of the radial force in two-body model to that in the ER3BP:

$$k = F_{mercury} / (F_{mercury} + F_{other}) = \mu_m / \mu_m^* \tag{16}$$

where $F_{mercury}$ represents the gravity of Mercury, F_{other} represents the radial components arising from other forces, and μ_m^* denotes the gravitational parameter in the ER3BP.

Then in the ER3BP the orbital eccentricity e_c^* is given by

$$e_c^* + 1 = \frac{{v_p}^2 \cdot r_p}{\mu_m^*} \tag{17}$$

From Eqs. 15 ~ 17, the relationship between e_c^* and e_c is

$$e_c^* + 1 = k(e_c + 1) \tag{18}$$

The reason why we establish the relationship between e_c^* and e_c is that capture eccentricity is important to capture. Small capture eccentricity represents a higher capture quality, because it implies small capture velocity and transient capture orbit closer to the circular orbit. Therefore the capture eccentricity can be used as an effective index to evaluate the quality of the gravitational capture.

Figure 4 shows the relationship between e_c^* and e_c for different k. The discussion about Eq. 18 is as follows.

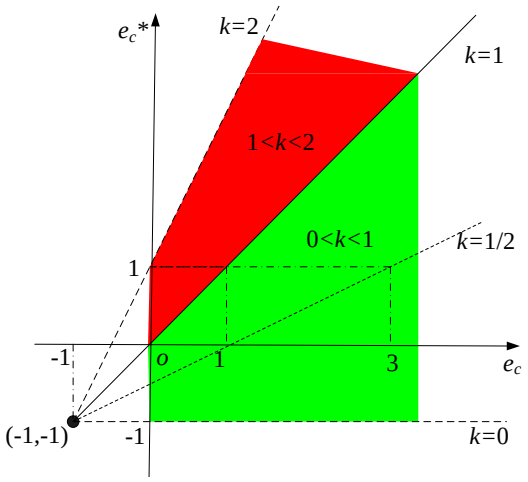

Figure 4. The relational graph between e_c^* and e_c

Figure 4 shows some useful information:

If k=1, e_c^* is equal to e_c. In this case the radial force from other forces $F_{other} = 0$.

If k>1, e_c^* is greater than e_c (the red region in Fig. 4), therefore, the capture effect in the ER3BP is inferior to that in two-body model. Especially let k=2, if 0< e_c <1, e_c^* is greater than 1, which means that the capture condition satisfied in two-body model cannot be satisfied in the ER3BP. This situation, of course, should be avoided. However, this situation is available for the gravitational escape. If k continues to increase, it is meaningless for the research in the ER3BP. Therefore, k=2 is an upper bound, and in this case $F_{other} = -F_{mercury}/2$.

If 0<k<1, e_c^* is less than e_c (the green region in Fig. 4). The capture effect in the ER3BP is superior to that in two-body model. For example, let k=1/2, if e_c <1, e_c^* is less than 0, which means that the capture point is apoherm; if 1< e_c <3, apparently the capture cannot be achieved in two-body model, whereas in the ER3BP e_c^* is less than 1, which can satisfy the criteria of the capture. In addition, the less k the better effect on the capture. However, k has a lower bound 0. Numerical methodology can help us to understand k and $\boldsymbol{a}_r^t$ more clearly. And some description about this methodology should be stated before computation.

In the mercury-centric rotating frame, the position $\boldsymbol{p}$ and the velocity $\boldsymbol{v}$ of any capture point can be determined by six orbital elements of transient capture orbit. Considering the capture point is periherm, if the orbital eccentricity e_c and the distance from periherm to the barycenter of Mercury r_p are given, in fact we just need the longitude of ascending node Ω, the orbit inclination i and the argument of periherm ω to describe the state of any capture point (see Fig.

5). When r_p is fixed, the spherical surface in Fig. 5 is called the sphere of capture, which consists of the capture points. The position $\boldsymbol{p}$ and the velocity $\boldsymbol{v}$ of capture point are given by

$$\boldsymbol{p} = \begin{bmatrix} \cos\omega\cos\Omega - \sin\omega\cos i\sin\Omega & -\sin\omega\cos\Omega - \cos\omega\cos i\sin\Omega & \sin i\sin\Omega \\ \cos\omega\sin\Omega + \sin\omega\cos i\cos\Omega & -\sin\omega\sin\Omega + \cos\omega\cos i\cos\Omega & -\sin i\cos\Omega \\ \sin\omega\sin i & \cos\omega\sin i & \cos i \end{bmatrix} \begin{bmatrix} r_p \\ 0 \\ 0 \end{bmatrix} \quad (19a)$$

$$\boldsymbol{v} = \begin{bmatrix} \cos\omega\cos\Omega - \sin\omega\cos i\sin\Omega & -\sin\omega\cos\Omega - \cos\omega\cos i\sin\Omega & \sin i\sin\Omega \\ \cos\omega\sin\Omega + \sin\omega\cos i\cos\Omega & -\sin\omega\sin\Omega + \cos\omega\cos i\cos\Omega & -\sin i\cos\Omega \\ \sin\omega\sin i & \cos\omega\sin i & \cos i \end{bmatrix} \begin{bmatrix} 0 \\ v_p \\ 0 \end{bmatrix} \quad (19b)$$

where v_p can be obtained from Eq. 15. The ranges of Ω, i and ω are from 0^o to 360^o, from 0^o to 180^o and from 0^o to 360^o, respectively.

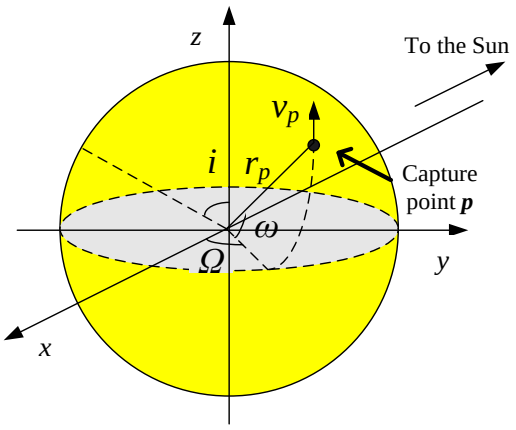

Figure 5. The sphere of capture described by the orbital elements in the mercury-centric rotating frame

Furthermore, even the longitude of ascending node Ω is given, the position $\boldsymbol{p}$ of any capture point can still be determined uniquely by the orbit inclination i and the argument of periherm ω. However, the variation of Ω will affect the direction of the capture velocity.

By these three orbital elements shown above, we obtain the position $\boldsymbol{p}$ and the velocity $\boldsymbol{v}$ of the capture point. Then we need to transform them into the Sun-Mercury nondimensional rotating frame in which they can be expressed as

$$\boldsymbol{\rho}_0 = (1-\mu)\boldsymbol{r} + \frac{\boldsymbol{p}}{r} \quad (20a)$$

$$\dot{\boldsymbol{\rho}}_0 = \frac{t_N}{r}\boldsymbol{v} - \dot{\theta}\eta_1\frac{\boldsymbol{p}}{r} \quad (20b)$$

where t_N is the unit time.

Then the Eq. 16 can be used to implement the numerical computation in the ER3BP. Figure 6 shows k on the sphere of capture described by i and ω, where r_p =2640 km (the height of periherm is 200 km), $e_c = 0.97$, $\Omega = 90^o$ and $\theta = 0^o$. Notice that the sphere of capture in Fig. 6 is described in the mercury-centric rotating frame.

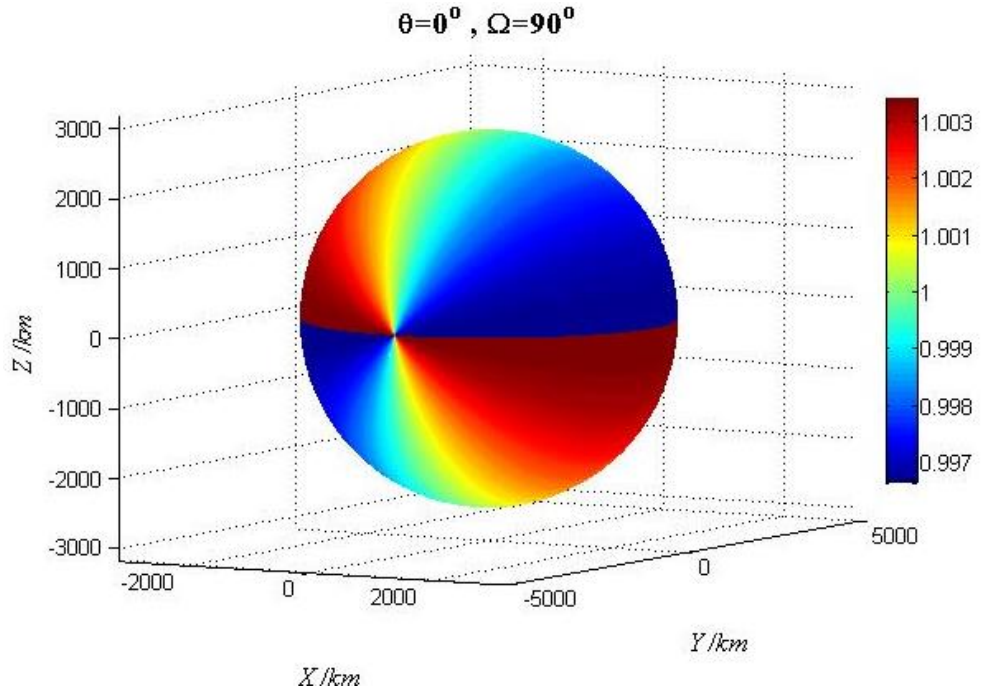

Figure 6. *k* on the sphere of capture where $\theta = 0^o$ and $\Omega = 90^o$

From Fig. 6, we find k on the sphere of capture is very close to 1 (the magnitude of the difference is about 10^{-3}). This result is in accordance with the fact that the gravitation of Mercury is dominant in the space near Mercury. However, k is variable slightly at different capture point. Figure 6 shows that the direct orbits ($0^o < i < 90^o$) possess the larger k and the retrograde orbits ($90^o < i < 180^o$) possess the smaller k. This phenomenon will explain some results obtained in Sect. 4.

Suppose that the height and the velocity magnitude of the capture point are given, i.e., r_p and e_c are fixed, then the influence parameters involved in the numerical computation only include the Mercury true anomaly θ and the longitude of ascending node Ω. From the analysis presented above, we know that Ω affects the velocity direction of capture point and the influences of θ appear in all of the parts. The detailed parameter analysis is shown in next subsection.

3.3. Parameter Analysis

Using the mechanics analysis in Sect.3.1, the parameter k can be defined as follows

$$k = \frac{F_{mercury}}{F_{mercury} + F_{other}} = \frac{F_{mercury}}{F_{mercury} + F_{sun} + F_{centrifugal} + F_{coriolis}} \qquad (21)$$

where F_{sun}, $F_{centrifugal}$ and $F_{coriolis}$ represent the radial force from the Sun, the centrifugal force and the Coriolis force, respectively. The radical forces related to the position of the capture point include $F_{mercury}$, F_{sun} and $F_{centrifugal}$. $F_{coriolis}$ is directly related to the velocity of the capture point. Considering F_{other} as small quantity compared with $F_{mercury}$ and neglecting the higher order terms, Eq. 21 can be expanded by

$$k = \left(1 + \frac{F_{other}}{F_{mercury}}\right)^{-1} \approx 1 - \frac{F_{other}}{F_{mercury}} = \left(1 - \frac{F_{sun} + F_{centrifugal}}{F_{mercury}}\right) - \frac{F_{coriolis}}{F_{mercury}} \qquad (22)$$

where $F_{coriolis}/F_{mercury}$ indicates the influence of Ω and the influences of θ are manifested in all terms of Eq. 22.

Considering r_p =2640 km, capture eccentricity $e_c = 0.97$, we study the effect of Ω and θ on k on the sphere of capture.

Firstly we demonstrate the influence of θ on k. Figure 7 shows k_{max} and k_{min}, the maximum and the minimum of k, with different θ and Ω. From Fig. 7, we find that k_{max} and k_{min} are mainly affected by the Mercury anomaly θ. Besides the magnitude of their variations is 10^{-3}, which is same as the magnitude of the difference of k (see Fig. 6). Therefore, we conclude that the influence of θ on the distribution of k on the sphere of capture cannot be negligible.

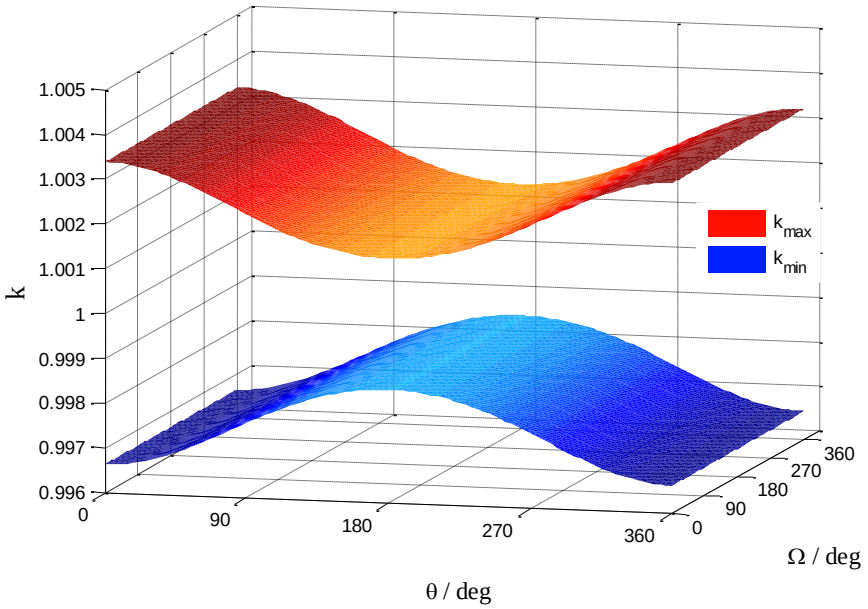

Figure 7. k_{max} **and** k_{min} **with different** θ **and** Ω

Secondly we demonstrate the influence of Ω. As r_p is fixed, $F_{mercury}$ is invariable. According to Eq. 13, we can calculate the maximum and minimum variations of $F_{coriolis}/F_{mercury}$. Figure 8 shows $(F_{coriolis}/F_{mercury})_{\max}$ and $(F_{coriolis}/F_{mercury})_{\min}$ with different θ and Ω. It is showed that the

variations of $F_{coriolis}/F_{mercury}$ possess the same magnitude of the difference k on the sphere of capture. According to Eq. 22, we conclude that the function of $F_{coriolis}/F_{mercury}$ is significant, i.e., the influence of Ω on the distribution of k on the sphere of capture also cannot be negligible.

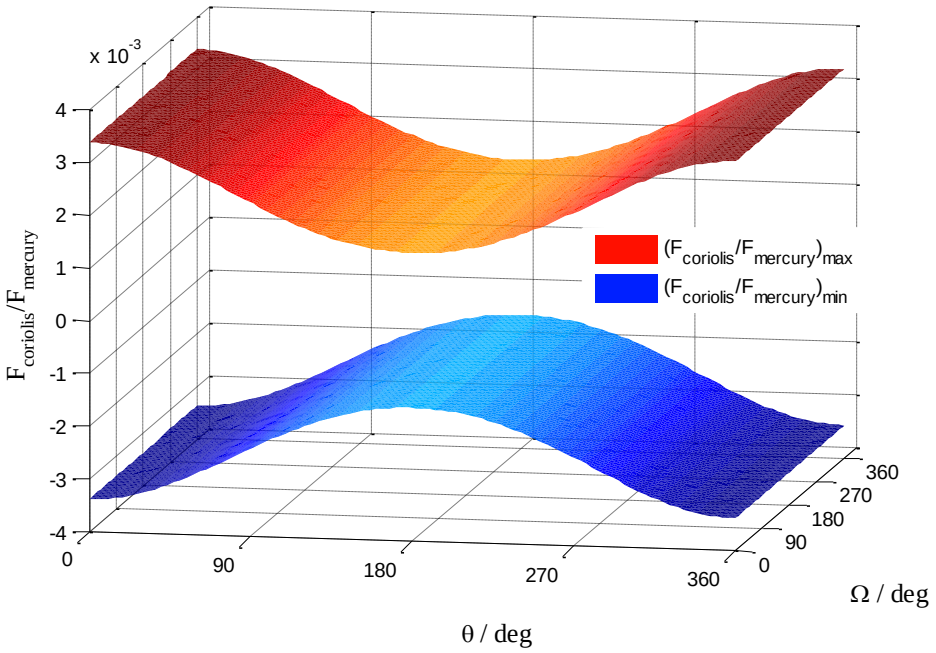

Figure 8. $(F_{coriolis}/F_{mercury})_{max}$ **and** $(F_{coriolis}/F_{mercury})_{\min}$ **with different** θ **and** Ω

At last, we analyze the influence of tangential force on the gravitational capture. Figure 9 shows the maximum and minimum of tangential acceleration a_r^t with different θ and Ω. Because the surfaces of the maximum and minimum of a_r^t are very close, they look like one surface. Figure 9 sheds light on a_r^t is mainly influenced by θ. Of particular concern is that no matter whether the maximum or the minimum, a_r^t is less than 0 where $0^o < \theta < 180^o$, while a_r^t is greater than 0 where $180^o < \theta < 360^o$. Therefore, we conclude that the tangential force is always the resistance when $0^o < \theta < 180^o$, and the tangential force is always the thrust when $180^o < \theta < 360^o$.

However, we find from Fig. 9, the magnitude of a_r^t is 10^{-2}. Considering the braking time Δt is also very small, the velocity increment $\Delta v = a_r^t \Delta t$ (a product of two small quantity) caused by the tangential acceleration is quite small. Therefore the effect of the tangential acceleration on the gravitational capture point is negligible.

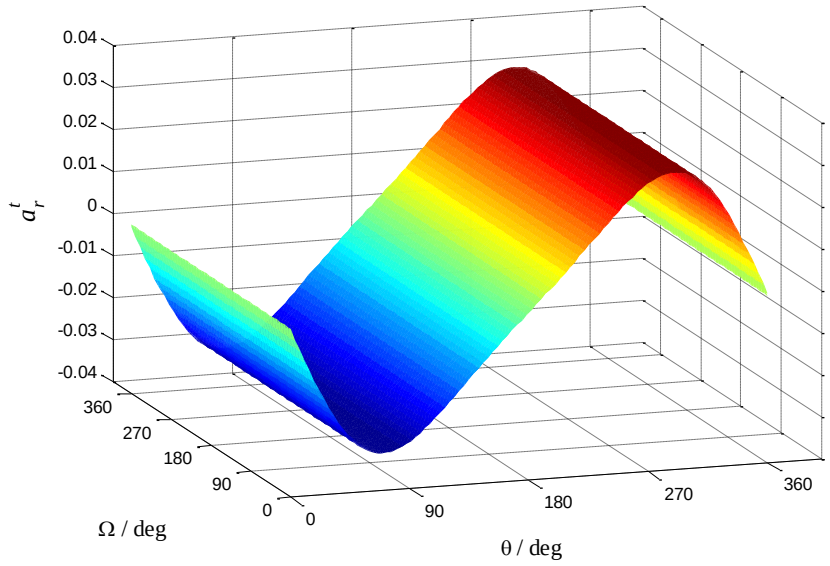

Figure 9. The maximum and minimum of a_r^t with different θ and Ω

4. Capture Eccentricity

Considering the request of the actual space mission, the time of flight cannot be too long. Because the longer the time of flight is, the more disturbances the spacecraft will suffer. Meanwhile the orbit control will become more complex and difficult. Therefore, we adopt the criteria of the gravitational capture: for the spacecraft, the time of flight from the boundary of the SOI (radius is 300000 km) to the capture point is restricted to 60 days. In this paper we regard the capture points (r_p =2640 km) as the initial values, the trajectories are numerically integrated backward in time in the ER3BP. If the spacecraft cannot reach the boundary of SOI within 60 days, we deem the gravitational capture cannot be achieved.

4.1. Minimum Capture Eccentricity

As we have analyzed in Sect 3.2, the less capture eccentricity e_c, the higher quality of the gravitational capture. Within the restriction of the time-of-flight, the state (includes the position and velocity direction) of each capture point has the unique minimum capture eccentricity $e_{\min}$ correspondingly. And $e_{\min}$ can help us evaluate the state of the capture point.

Numerical calculation for $e_{\min}$ is as follows and the description of the methodology is same as Sect 3.2. Figure 10 displays the distribution of the minimum capture eccentricity $e_{\min}$ on the sphere of capture, where $\theta = 90^{\circ}$ and $\Omega = 0^{\circ}$.

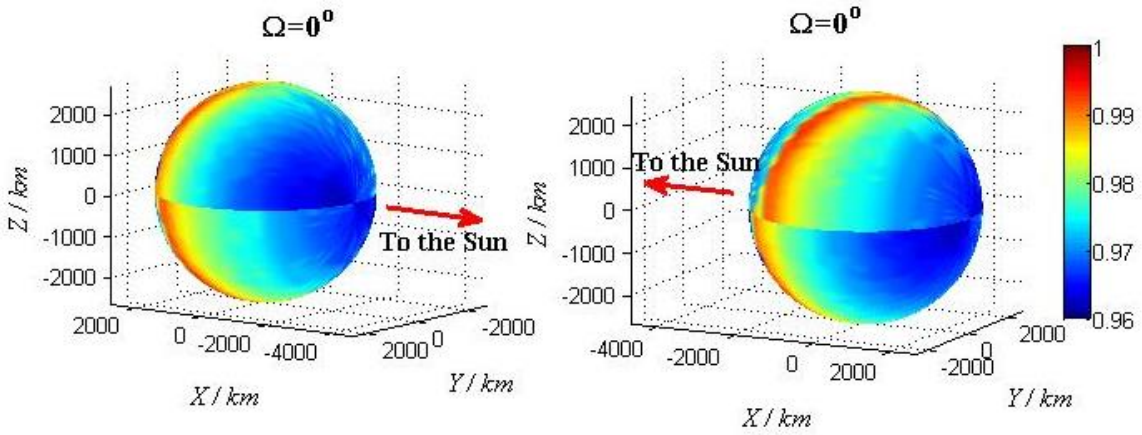

Figure 10. The minimum capture eccentricity $e_{\min}$ on the sphere of capture

Because the radius of capture point r_p is fixed, there are only two parameters that can affect the distribution of $e_{\min}$, i.e. Ω and θ. We firstly discuss the effect of θ. By comparing numerical results, we find that the effect of θ on the distribution of $e_{\min}$ is significant. Limited by space, here only a part of numerical results is demonstrated. Let $\Omega = 90^{o}$, Fig.11 shows the distribution of the minimum capture eccentricity $e_{\min}$ in $i-\omega$ coordinate system, if θ are 0^{o}, 90^{o}, 180^{o} and 270^{o}, respectively.

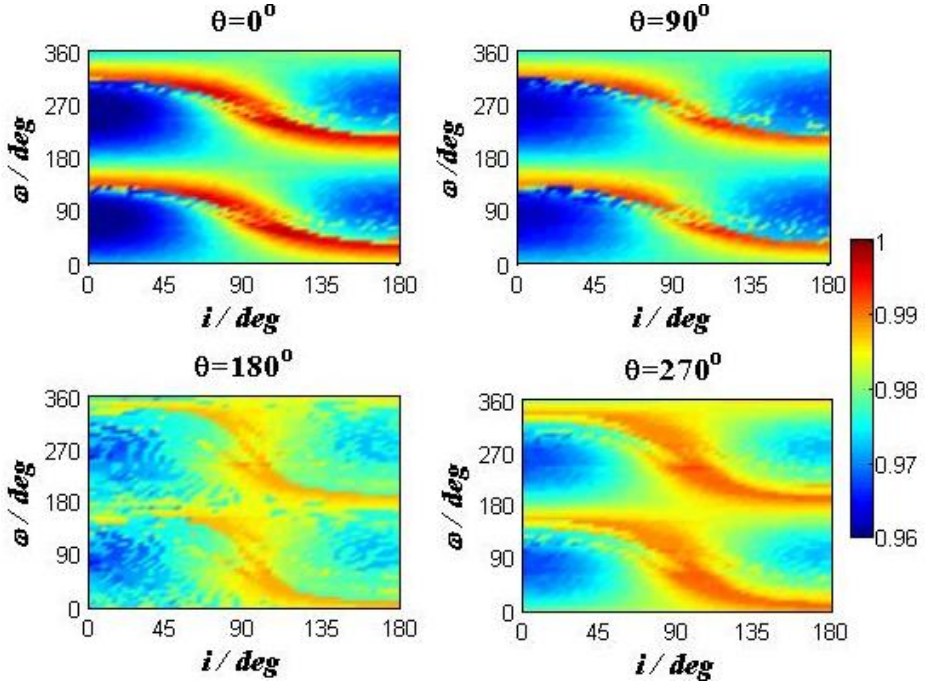

Figure 11. The minimum capture eccentricity $e_{\min}$ in $i-\omega$ coordinate system

Figure 11 sheds light on the influence of θ on the distribution of $e_{\min}$. Of particular concern are the dark blue regions in Fig.11. Those special regions represent the global minimum $e_{\min}$, which

means the optimal effect of the gravitational capture. As we can see from Fig. 11, if θ is 0^{o}, the dark blue regions are large and complete; if θ is 180^{o}, the dark blue regions are small and fragmented; the situations of 90^{o} and 270^{o} are intermediate. Therefore, when Mercury is at the vicinity of perihelion, the gravitational capture is easier. On the contrary, the condition of aphelion is more detrimental to the gravitational capture. In order to detect the influence of θ more clearly, we plot $e_{\min}$ with different θ (see Fig. 12). We choose the capture points from the dark blue regions in Fig. 11 as the initial values, and suppose ω is set as 270^{o}.

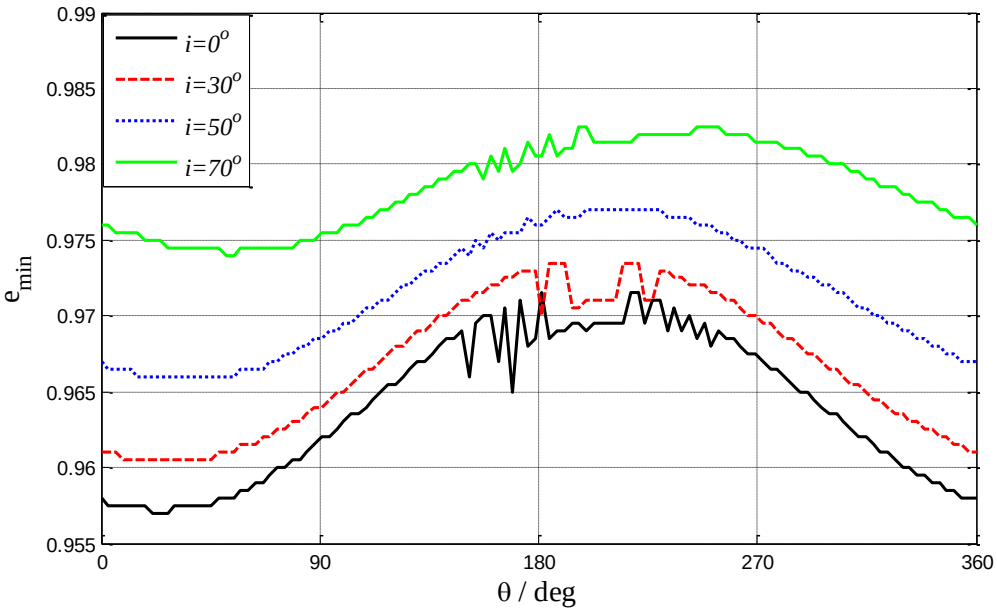

Figure 12. $e_{\min}$ **with different** θ **and** i

As we can see from Fig.12, no matter what i is chosen as, when θ is near 0^{o}, $e_{\min}$ becomes smaller; when θ is near 180^{o}, $e_{\min}$ becomes greater. The situation of $i = 0^{o}$ is the most significant among the curves, because $e_{\min}$ is the lowest in that case. Actually if i is equal to 0^{o}, Figure 12 illustrates 0^{o} is not the optimal for θ. When θ is about $30^{o} \sim 40^{o}$, the corresponding $e_{\min}$ is minimal, which is a little less than the situation of $\theta = 0^{o}$.

Figure 11 shows the dark blue regions are distributed on where $0^{o} < i < 45^{o}$, and ω is about 70^{o} or 250^{o}. Those, in fact, are the near-Sun side and far-Sun side on the sphere of capture along the x axis. Figure 10 likewise reflects the near-Sun region and far-Sun region exist the global minimum $e_{\min}$. As a consequence we will focus on those two special regions (see Fig. 13).

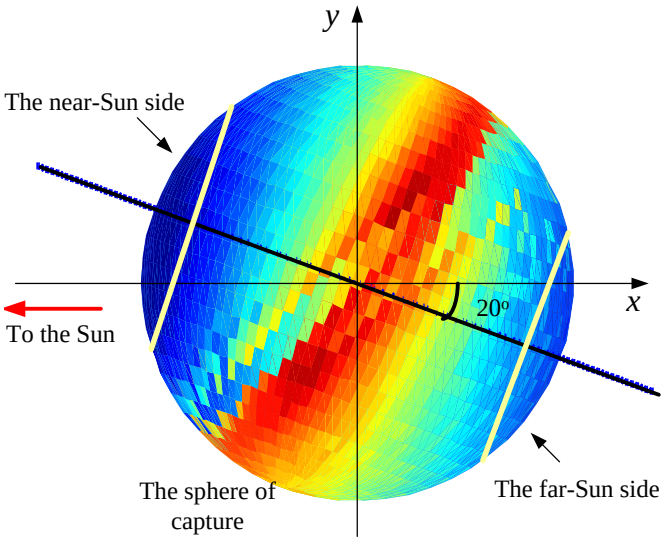

Figure 13. The special regions on the sphere of capture

Figure 13 shows two special regions, i.e. the near-Sun region and far-Sun region. As we can see, those two regions are not symmetrical with respect to x axis. The deviation is about 20^{o}. Thus, to make the special regions symmetrical, we choose Ω are -20^{o}, 70^{o}, 160^{o} and 250^{o} respectively in the following numerical calculation. In addition, in order to study the optimal condition for the gravitational capture, we suppose θ is 0^{o} (in fact $30^{o} \sim 40^{o}$ is optimal for θ, but the difference between them is very slight) based on the previous analysis.

Figures 14 and 15 show the distribution of $e_{\min}$ on the sphere of capture. Figure 14 is the image of the near-Sun side, which is viewed along the x axis. Figure 15 is the image of the far-Sun side, which is viewed against the x axis. The yellow arrows in the dark blue regions indicate the velocity direction of capture points.

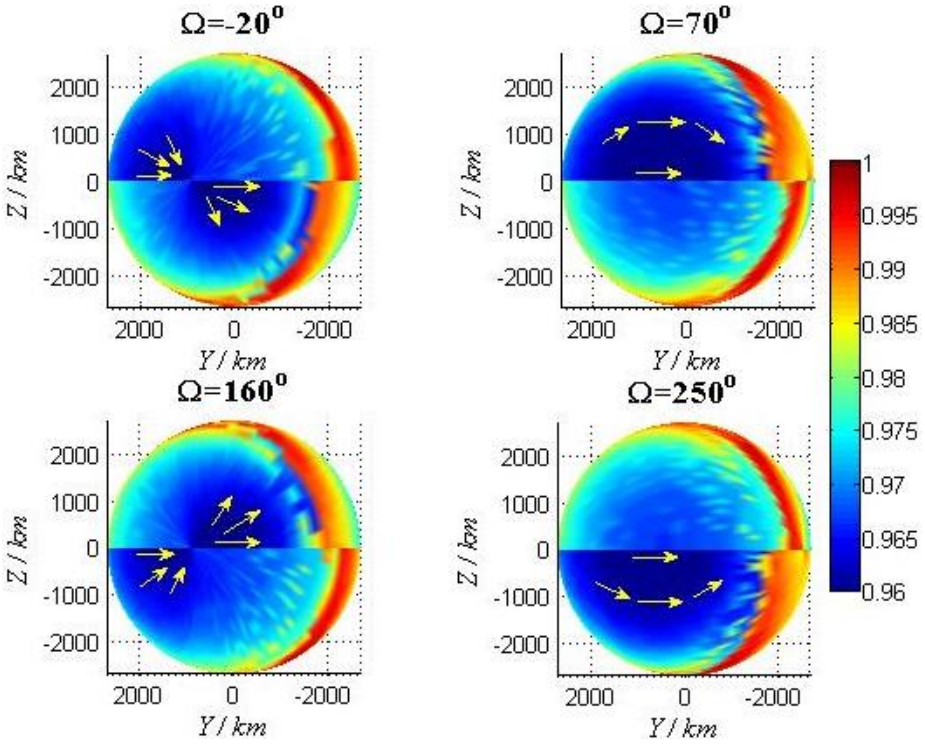

Figure 14. The distribution of $e_{\min}$ on the near-Sun side

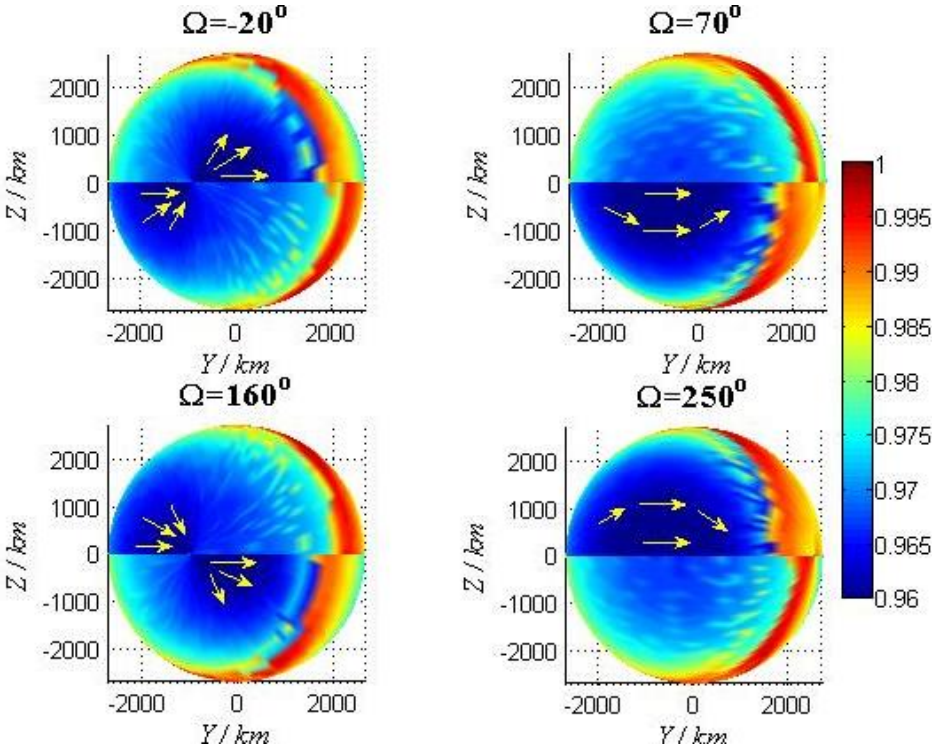

Figure 15. The distribution of $e_{\min}$ on the far-Sun side

Summarizing the dark blue regions, we can get the distribution of the global minimum $e_{\min}$ on the sphere of capture. For these regions we have following conclusion:

1. There are two special regions, which are umbrella-shaped and locate in the near-Sun side and the far-Sun side of the sphere of capture (see Fig. 13).

2. Only the direct orbit in those special regions corresponds to the global minimum $e_{\min}$.

From Sect. 3.2, we know that the direct orbit possesses the larger *k*, which denotes the smaller radical force. It will be easier to escape (that is to be captured in the forward propagation). Hence the second conclusion can be explained.

4.2. Corrected Minimum Capture Eccentricity

According to Sect 3.2, we can also utilize the given state of capture point and eccentricity to correspondingly derive the corrected ratio of the radial force *k*. Then we can use Eq. 18 to obtain the corrected minimum capture eccentricity $e^*_{\min}$ corresponding to the state of the capture point in the ER3BP. $e^*_{\min}$ integrates the mechanical information of the capture point into $e_{\min}$ and can be regarded as another index of the gravitational capture. Numerical calculation for $e^*_{\min}$ is performed as follows.

Let $\theta = 0^o$, Figures 16 and 17 show the distribution of $e^*_{\min}$ on the sphere of capture, where Ω are 0^o, 90^o, 180^o and 270^o, respectively. Figure 16 is the image of the near-Sun side. Figure 17 is the image of the far-Sun side. The yellow arrows in the dark blue regions indicate the velocity direction of capture points.

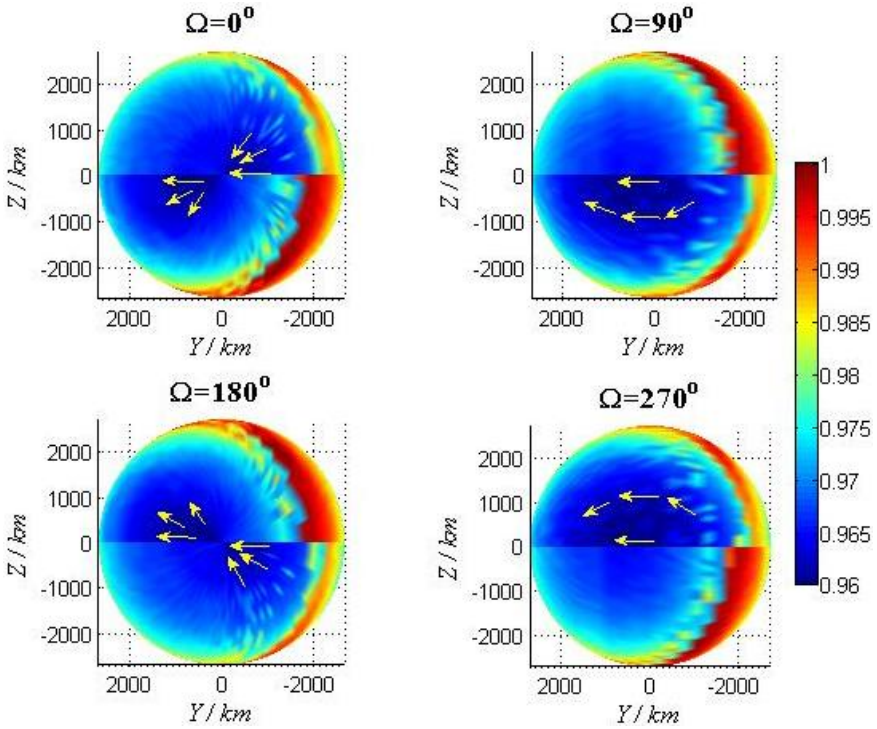

Figure 16. The distribution of $e^*_{\min}$ on the near-Sun side

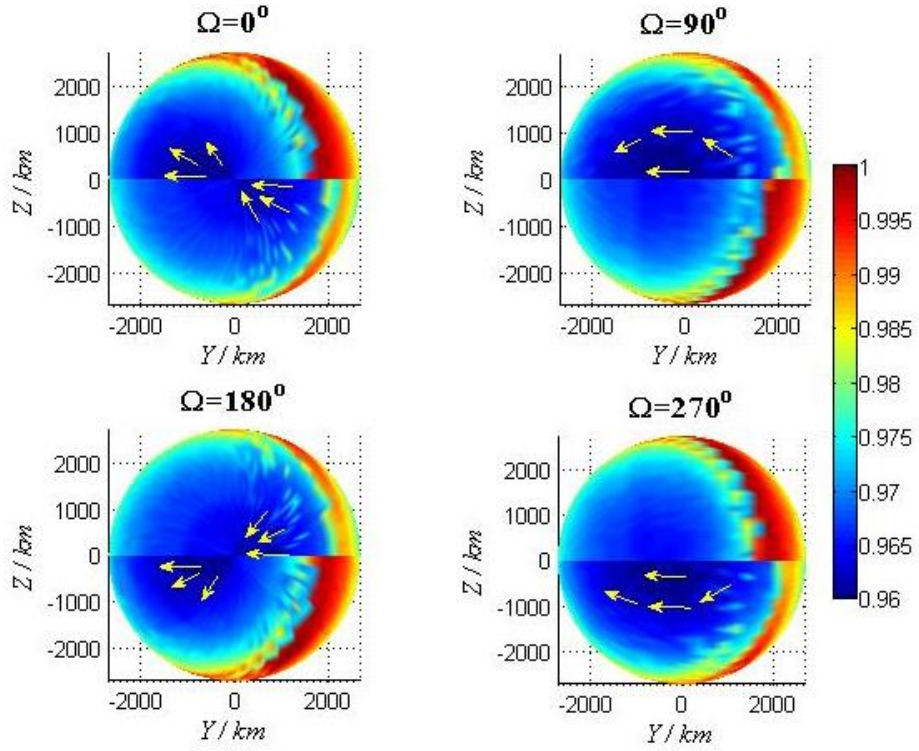

Figure 17. The distribution of $e^*_{\min}$ on the far-Sun side

As we can see from Figures 16 and 17, the dark blue regions are the special regions, where the global minimum $e^*_{\min}$ exists. There are still two special regions, which locate in the near-Sun side and the far-Sun side of the sphere of capture. However, comparing with Figures 14 and 15, the distribution of $e^*_{\min}$ on the sphere of capture is different from $e_{\min}$. Specifically, only the retrograde orbit in those special regions can correspond to the global minimum $e^*_{\min}$. Let's recall a conclusion in Sect. 3.2: the retrograde orbits possess the smaller *k*. For the same $e_{\min}$, the less *k* the less $e^*_{\min}$. This fact can explain why the retrograde orbit in those special regions corresponds to the global minimum $e^*_{\min}$.

5. Trajectory Design

As an application of the previous results, in this subsection, the design of the gravitational capture trajectory will be investigated.

From the conclusions in Sect. 4, we know there exist two special regions on the sphere of capture, in which the capture point possesses the global minimum $e_{\min}$ and $e^*_{\min}$. Therefore we can choose some capture points from the inside of those regions as the initial values. Then by backward and forward integration, we can get the corresponding capture trajectories.

Firstly $e_{\min}$ is considered. Figure 18 shows a gravitational capture trajectory described in the nondimensional Sun-Mercury rotating frame.

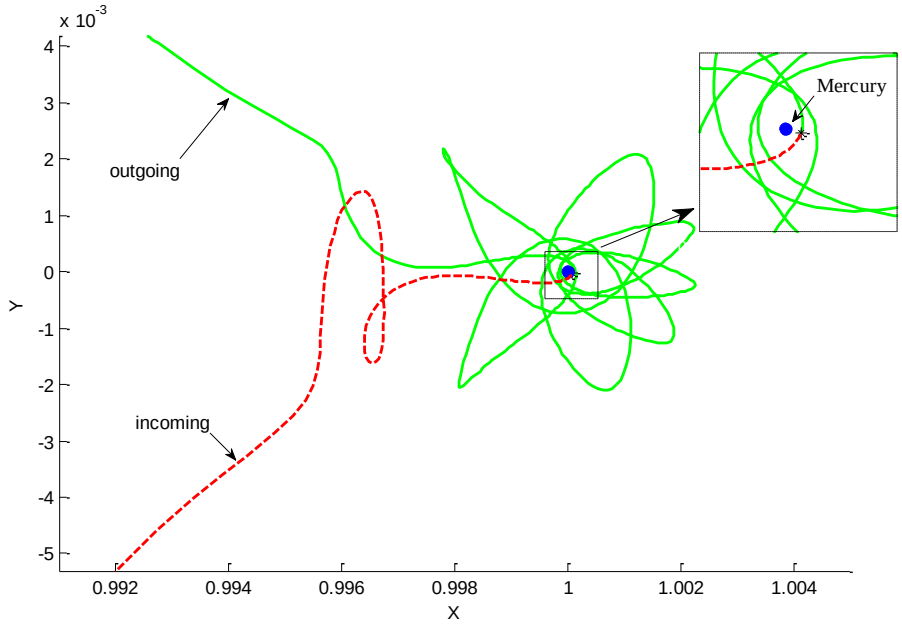

Figure 18. A gravitational capture trajectory without braking

In Fig. 18, the capture point is chosen from the dark blue regions of Fig. 11, where θ is 0^{o} and Ω is 90^{o}. The other parameters are set as: $e_{\min} = 0.941698$, $i = 0^{o}$ and $\omega = 250^{o}$. The black "*" mark denotes the capture point, the red dash line denotes the incoming trajectory from the outside of the SOI and the green solid line denotes the outgoing trajectory from the region of Mercury. Obviously, Fig. 18 shows the gravitational capture is temporary capture, after some revolutions the spacecraft finally fly away from the vicinity of Mercury. Then braking is necessary to accomplish permanent capture. If we take brake at capture point, where Δv is 0.3699m/s in the opposite direction to the motion, the spacecraft can stay in the region of Mercury within 250 days (see Fig. 19). Then we almost regard the capture as long-term capture.

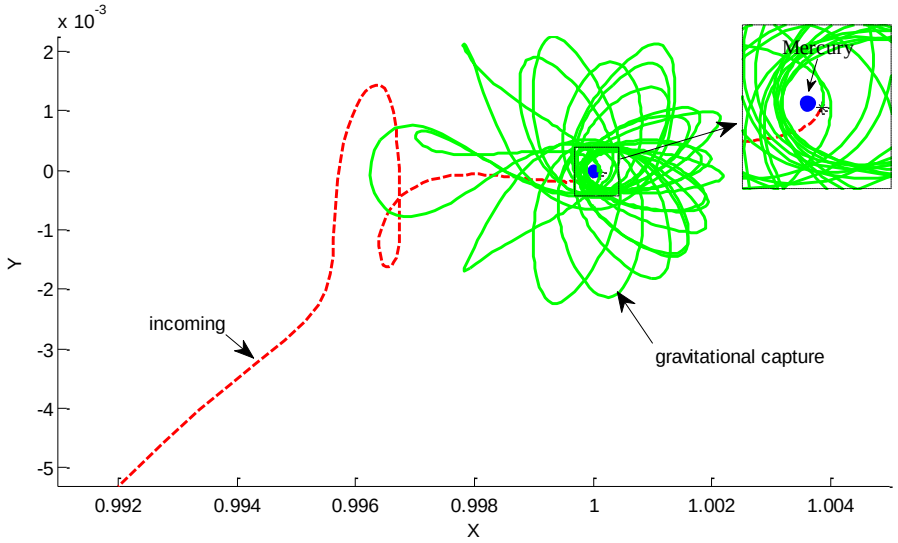

Figure 19. A gravitational capture trajectory with braking

Then $e^*_{\min}$ is considered. We choose the capture point from the dark blue regions in Fig. 17, where Ω is 90^o and θ is 0^o. The other parameters are set as: $e^*_{\min} = 0.947522$, i =180^o and ω=280^o. The trajectory is showed in Fig. 20. The black "*" mark denotes capture point, the red dash line denotes the incoming trajectory from the outside of the SOI and the green solid line denotes the section after the gravitational capture. As we can see from Fig. 20, even though the braking is not conducted at the capture point, the spacecraft still remain in the region of Mercury within 250 days. We can calculate that $e_{\min}$ of the capture point in this situation is 0.954066, which is a little larger than that in the situation of Fig. 19. But the fuel consumption in Fig. 20 is zero. Therefore the special regions of $e_{\min}$ and $e^*_{\min}$ have both advantages and disadvantages. The radius of Mercury in particular is not considered in Fig. 20. Actually, the spacecraft has crashed into the Mercury after some revolutions. This fact can be used in the trajectory design of some intercept missions, such as Deep impact mission.

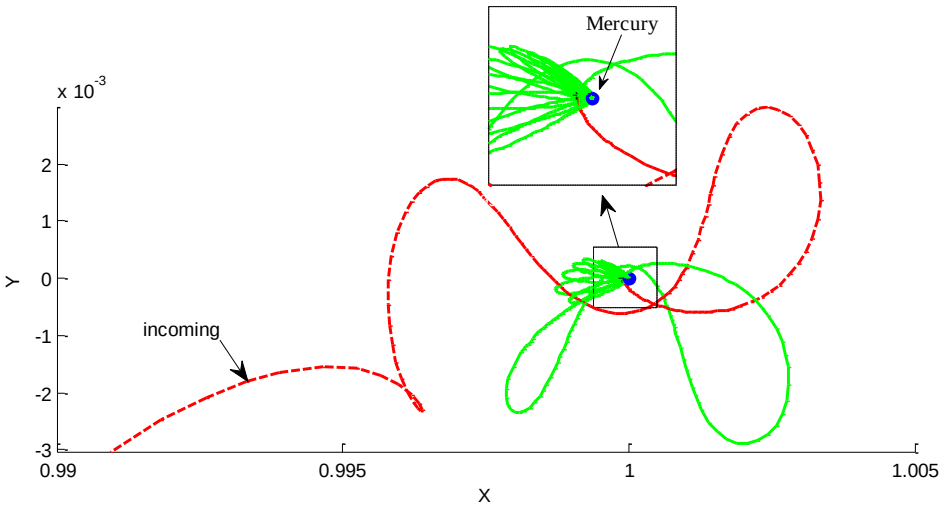

Figure 20. A gravitational capture trajectory without braking

6. Conclusions

In this paper, the gravitational capture at Mercury has been investigated under the frame of Sun-Mercury-spacecraft ER3BP. A new parameter *k*, the corrected ratio of the radial force, was proposed to establish the relationship between capture eccentricity e_c in two-body model and capture eccentricity e^*_c in the ER3BP. Numerical methodology revealed the influences of the parameters on the distribution of *k* and tangential force on the sphere of capture.

Under the restriction of the time-of-flight and corrected ratio *k*, the minimum capture eccentricity $e_{\min}$ and the corrected minimum capture eccentricity $e^*_{\min}$ were proposed respectively as indexes to evaluate the quality of the gravitational capture in the ER3BP. Numerical calculation showed that when Mercury was at the vicinity of perihelion, the gravitational capture was easier. Besides, the capture points in the near-Sun side and the far-Sun side of the sphere of capture possessed the global minimum $e_{\min}$ and $e^*_{\min}$. The direct and retrograde orbit in these region respectively

corresponded to the global minimum $e_{\min}$ and $e^*_{\min}$. At last, the results were used to design the gravitational capture trajectories. We find that $e_{\min}$ and $e^*_{\min}$ have both advantages and disadvantages as indexes to evaluate the capture point.

The methods and results presented in this paper are made for the Sun-Mercury-Spacecraft system, but actually they can also be valid for any system of primaries.

7. References

[1] Belbruno, E.A. "Capture Dynamics and Chaotic Motions in Celestial Mechanics: With Applications to the Construction of Low Energy Transfers." Princeton Univ. Press, Princeton, NJ, pp. 111–114, 145–150, 2004.

[2] Schoenmaekers, J., Horas, D., and Pulido, J.A. "SMART-1 with Solar Electric Propulsion to the Moon." Proceeding 16th International Symposium on Space Flight Dynamics –16th ISSFD. Pasadena, CA, 2001.

[3] Roncoli, R.B., and Fujii, K.K. "Mission Design Overview for the Gravity Recovery and Interior Laboratory (GRAIL) Mission." AIAA/AAS Astrodynamics Specialist Conference, Toronto, August, 2010.

[4] Jehn, R., Campagnola, S., Garc á, D., and Kemble, S. "Low-Thrust Approach and Gravitational Capture at Mercury." Proceedings 18th International Symposium on Space Flights Dynamics –18th ISSFD., Vol. 584, ESA, Noordwick, The Netherlands, pp. 487, 2004.

[5] Belbruno, E.A. "Lunar Capture Orbits, A Method of Constructing Earth Moon Trajectories and the Lunar Gas Mission." AIAA-87-1054. In: 19th AIAA/DGLR/JSASS International Electric Propulsion Conference, Colorado Springs, CO, May, 1987.

[6] Belbruno, E.A. "Examples of the Nonlinear Dynamics of Ballistic Capture and Escape in the Earth–Moon System." AIAA-90-2896. In: AIAA Astrodynamics Conference, Portland, OR, August, 1990.

[7] Belbruno, E.A. "Ballistic Lunar Capture Transfer Using the Fuzzy Boundary and Solar Perturbations: a survey." In: Proceedings for the International Congress of SETI Sail and Astrodynamics, Turin, Italy, 1992.

[8] Belbruno, E.A., and Miller, J.K. "A Ballistic Lunar Capture Trajectory for Japanese Spacecraft Hiten." Jet Propulsion Lab., JPL IOM 312/90.4-1731, Internal Document, Pasadena, CA, June, 1990.

[9] Krish, V., Belbruno, E.A., and Hollister, W.M. "An Investigation into Critical Aspects of a New Form of Low Energy Lunar Transfer, the Belbruno-Miller Trajectories." Proceedings of the AIAA/AAS Astrodynamics Conference, AIAA, Washington, DC, pp. 435–444. 1992.

[10] Neto, V. E., and Prado, A. F. B. A. “Time-of-Flight Analyses for the Gravitational Capture Maneuver.” Journal of Guidance, Control, and Dynamics, Vol. 21, No. 1, pp. 122–126. 1998.

[11] Machuy, A.L., Prado, A.F.B.A., and Stuchi, T.J. “Numerical Study of the Time Required for the Gravitational Capture in the Bi-circular Four-Body Problem.” Advances in Space Research 40, pp. 118–124. 2007.

[12] Fantino, E., Gomez, G., Masdemont, J.J., Ren, Y. “A Note on Libration Point Orbits, Temporary Capture and Low-Energy Transfers.” Acta Astronautica 67. pp. 1038–1052. 2010.

[13] Prado, A.F.B.A. “Numerical and Analytical Study of the Gravitational Capture in the Bicircular Problem.” Advances in Space Research 36, pp. 578–584. 2005.

[14] Circi, C., and Teofilatto, P. “Effect of Planetary Eccentricity on Ballistic Capture in the Solar System.” Celestial Mechanics and Dynamical Astronomy 93, pp. 69–86. 2005.

[15] Prado, A.F.B.A, and Neto, V. E. “Study of the Gravitational Capture in the Elliptical Restricted Three-Body Problem.” The Journal of the Astronautical Sciences, Vol. 54, Nos. 3 & 4, pp. 567–582. July–December, 2006.

[16] Hyeraci, N, and Topputo, F. “Method to Design Ballistic Capture in the Elliptic Restricted Three-Body Problem.” Journal of Guidance, Control, and Dynamics, Vol. 33, No. 6, pp. 1814-1823. November–December, 2010.

[17] Bate, R.R., Mueller, D.D., and White, J.E. “Fundamentals of Astrodynamics.” New York: Dover Publications. pp. 333–334. 1971.

[18] Hamilton, D.P., and Burns, J.A. “Orbital Stability Zones about Asteroids. II- The Destabilizing Effects of Eccentric Orbits and of Solar Radiation.” Icarus 96, pp. 43-64. 1992